15th AIAA/CEAS Aeroacoustics Conference (30th AIAA Aeroacoustics Conference)
11 - 13 May 2009, Miami, FL

AIAA 2009-3409

Influence of the nozzle-exit boundary-layer thickness on the flow and acoustic fields of initially laminar jets

Christophe Bogey* and **Christophe Bailly†**
Laboratoire de Mécanique des Fluides et d'Acoustique
UMR CNRS 5509, Ecole Centrale de Lyon
69134 Ecully, France

Round jets originating from a pipe nozzle are computed by Large-Eddy Simulations (LES) to investigate the effects of the nozzle-exit conditions on the flow and sound fields of initially laminar jets. The jets are at Mach number 0.9 and Reynolds number 10^5, and exhibit exit boundary layers characterized by Blasius velocity profiles, maximum root-mean-square axial velocity fluctuations between 0.2% and 1.9% of the jet velocity, and momentum thicknesses varying from 0.003 to 0.023 times the jet radius. The far-field noise is determined from the LES data on a cylindrical surface by solving the acoustic equations. Jets with thinner boundary layer develop earlier but at a slower rate, yielding longer potential cores and lower centerline turbulent intensities comparing well with measurements at high Reynolds numbers. In all jets the shear-layer transition is dominated by vortex rolling-ups and pairings, which generate strong components in the noise spectra. Just adding random disturbances of low magnitude in the nozzle however leads to weaker rolling-up and pairing processes, thus significantly reducing their contributions to the sound field. This high sensitivity to the initial conditions is in good agreement with experimental observations.

I. Introduction

Since many experimental works conducted during the seventies including, among others, those by Maestrello and McDaid,[1] Grosche[2] and Hill *et al.*,[3] it has been well known that the flow development and the acoustic characteristics of axisymmetric jets strongly depend on the properties of the nozzle-exit boundary layer. In jet studies, parameters such as the momentum thickness of the velocity profile, the levels of velocity fluctuations, as well as the laminar or turbulent state of the boundary layer, have thus to be considered, because their variations may noticeably modify turbulent mixing and noise generation features. Unfortunately they have been neither controlled nor documented in most experiments, except in some few works.[4–9] In round jets of radius r_0, Zaman[7,8] measured for instance an initial shear-layer momentum thickness of $\delta_\theta = 0.008r_0$ and negligible turbulent intensities at a diameter-based Reynolds number $\mathrm{Re}_D = 7 \times 10^4$, but $\delta_\theta = 0.004r_0$ and root-mean-square (rms) axial velocity fluctuations close to ten per cent of the jet velocity at $\mathrm{Re}_D = 2.5 \times 10^5$. In the same way, Bridges and Hussain[9] reported in jets at $\mathrm{Re}_D = 1.4 \times 10^5$ and 3.2×10^5 nozzle-exit momentum thicknesses $\delta_\theta = 0.005r_0$ and $0.003r_0$ and peak rms axial velocity fluctuations of 0.5% and 1.9%, respectively.

A difficulty in experiments aiming at studying the effects of initial conditions is that the inflow parameters cannot usually be changed independently, except for some very careful investigations such as those by Hussain and Zedan.[4,5] To distinguish the influence of jet inflow parameters, it then appears natural to perform numerical simulations. Works have been carried out to this end by Stanley and Sarkar,[10] Bogey and Bailly,[11] Bogey *et al.*,[12] and by Kim and Choi.[13] However, some questions remain because the computing limitations have led to differences between experimental and numerical inflow conditions, as specially pointed out in the reviews by Colonius and Lele[14] and by Bodony and Lele.[15] Regarding the initial shear-layer momentum

*CNRS Research Scientist, AIAA Member, christophe.bogey@ec-lyon.fr
†Professor at Ecole Centrale de Lyon & Institut Universitaire de France, Senior AIAA Member, christophe.bailly@ec-lyon.fr

thickness, values of $\delta_\theta = 0.016r_0$ and $\delta_\theta = 0.011r_0$ were for instance specified in Bogey *et al.*[12] and in Kim and Choi,[13] respectively, which is significantly higher than the experimental values mentioned above. The use of artifically thickened shear layers in jet simulations have resulted in some discrepancies with respect to the measurements. Shorter potential core lengths and higher sound pressure levels have in particular been observed in most computations.

According to experimental results, the influence of the initial shear-layer thickness on subsonic jet noise should however depend on the state of the turbulence at the nozzle exit. The variations of far-field noise features with the exit boundary-layer thickness can be expected to be stronger in initially laminar jets than in initially turbulent jets, namely tripped jets and jets at sufficiently high Reynolds numbers. Jets exhibit indeed laminar initial state for Reynolds numbers lower than a threshold value, which is around $\mathrm{Re}_D = 10^5$ from the analysis by Crighton[16] based on a set of experimental data. In the untripped jets of Zaman[7,8] for example, the flows were initially laminar for $\mathrm{Re}_D \leq 2.5 \times 10^5$. In such flows, rolling-ups and pairings of coherent vortical structures dominate the turbulent development in the first few diameters downstream of the nozzle. Because vortex pairings are efficient noise generators, intially laminar jets thus emit additional noise components with respect to initially turbulent jets.[1,2,7–9,12] In practice bumps are observed in the sound pressure spectra, especially for wide radiation angles for which noise is attributed to the turbulent scales developing randomly in the jets.[17–19] This extra noise, hence jet noise features, will be naturally affected by variations of the exit boundary-layer thickness through direct modifications of vortex pairing frequencies and strengths.

In the present study, the influence of the nozzle-exit boundary-layer thickness in initially laminar round jets is investigated by performing Large-Eddy Simulations (LES) combining low-dissipation and low-dispersion schemes and relaxation filtering for dissipating subgrid-scale energy. The acoustic far field radiated by the jets are calculated from the LES near field by solving the linear acoustic equations. The jets are isothermal, and at Mach number 0.9 and Reynolds number 10^5. To get closer to the experiments, a part of a pipe nozzle is included in the computational domain, and laminar boundary-layer profiles of thicknesses between $\delta = 0.025r_0$ and $\delta = 0.2r_0$ are imposed at the nozzle inlet. In first simulations, no disturbance is added in the pipe nozzle. The influence of the nozzle-exit momemtum thickness δ_θ will thus be examined in initially fully laminar jets, down to typical experimental values. The results will allow us in particular to examine whether simulations can reproduce the sensitivity to the initial conditions found in experiments, and also to discuss whether specifying very thin boundary layers in computations is sufficient to predict jet flow and noise features corresponding to those encountered in practical jets at high Reynolds numbers. In two additional simulations, random disturbances of low amplitude are added in the jet nozzle to investigate the effects of small variations of the exit turbulence, especially on the early stage of the shear-layer transition and on the radiated noise. In this way, we should be able to exhibit in the present paper the way in which changing δ_θ or the turbulent conditions at the nozzle exit modifies the noise contribution due to vortex pairings in the shear layer.

The paper is organized as follows. In section II, the parameters of the jet LES and of the extrapolation of the LES near field to the far field, including numerical algorithm, computational grids and times, are documented. The initial conditions of the jets, as well as the flow conditions at the pipe exit, are also presented. Some jet experiments whose results will be compared with the LES data and trends are finally reported in that section. In section III, vorticity and pressure snapshots are first shown. The shear-layer transitions, the overall flow developments and the acoustic far fields obtained for the different jets are then described in detail. Concluding remarks are provided in section IV. Finally, the coefficients used for a non-centered filter are provided in appendix.

II. Simulation parameters

A. Jet definition

Circular isothermal jets at Mach number $\mathrm{M} = u_j/c_a = 0.9$ and at Reynolds number $\mathrm{Re}_D = u_j D/\nu = 10^5$, originating from a pipe nozzle of radius r_0 and length $1.1r_0$, are computed by Large-Eddy Simulationn (u_j is the jet inflow velocity, c_a is the speed of sound in the ambient medium, $D = 2r_0$ is the nozzle diameter, and ν is the kinematic molecular viscosity). The ambient temperature and pressure are 293 K and 10^5 Pa. At the exit section of the nozzle at $z = 0$, the width of the nozzle lip is $0.053r_0$. At the pipe inlet at $z = -1.1r_0$, laminar Blasius boundary layers of thickness δ are imposed. The profiles of axial velocity u_z are

more precisely given by a polynomial approximation of the Blasius profile in the following way

$$u_z(r) = u_j \frac{r_0 - r}{\delta} \left[2 - 2 \left(\frac{(r_0 - r)}{\delta} \right)^2 + \left(\frac{r_0 - r}{\delta} \right)^3 \right] \quad \text{if} \quad r \geq r_0 - \delta$$

$$u_z(r) = u_j \quad \text{if} \quad r < r_0 - \delta$$

where r is the distance from the jet centerline. In addition, radial and azimuthal velocities are initially set to zero, pressure is kept constant to the ambient pressure, and the temperature is determined by a Crocco-Busemann relation.

Four jets characterized by inlet boundary-layer thicknesses $\delta = 0.025r_0$, $0.05r_0$, $0.1r_0$ and $0.2r_0$, referred to as JetD0025, JetD005, JetD01 and JetD02, are simulated as reported in table 1. To better match experiments, two additional jets with initial boundary-layer thickness $\delta = 0.05r_0$ are calculated. In these two cases JetD005p250 and JetD005p2000, unlike the four previous jets in which no forcing is applied in the nozzle, random pressure disturbances are introduced in the pipe within the boundary layer between $z = -0.4r_0$ and $z = -0.2r_0$. They are of maximum amplitude 250 and 2000 Pa, respectively. Finally, in order to seed the turbulent transition at the beginning of the simulations, random pressure fluctuations of maximum amplitude 200 Pa are added in the shear layer between $z = 0.25r_0$ and $z = 4r_0$ up to non-dimensional time $t = 18.75D/u_j$ in the six jet LES.

Table 1. Thickness of the inlet Blasius boundary layer δ, maximum amplitude of possible random pressure disturbances in the pipe, and line types used in the plots.

Reference	δ/r_0	Inlet random noise	Line type
JetD02	0.2	-	———
JetD01	0.1	-	– – –
JetD005	0.05	-	———
JetD0025	0.025	-	– – –
JetD005p250	0.05	250 Pa	———
JetD005p2000	0.05	2000 Pa	– – –

B. LES procedure and parameters

The LES is performed using a solver of the three-dimensional filtered compressible Navier-Stokes equations developed in cylindrical coordinates (r, θ, z) using low-dissipation and low-dispersion finite-difference schemes. The axis singularity is taken into account by the method proposed by Mohseni and Colonius.[20] Fourth-order eleven-point centered finite differences are used for spatial discretization, and a second-order six-stage low-storage Runge-Kutta algorithm is implemented for time integration.[21] To circumvent the severe time-step restriction induced by the cylindrical coordinates, the derivatives in the azimuthal direction around the axis are calculated using every n-th grid point, from $n = 2$ up to $n = 32$ at the closest points to the axis. To remove grid-to-grid oscillations, a sixth-order eleven-point centered filtering designed to only damp the shortest waves discretized[22] is applied every time step to the flow variables. The discretization at the boundaries is also taken into account by non-centered finite differences and filters with properties optimized in the Fourier space[23] (see in appendix the coefficients of a modified non-centered filter). The filtering is also employed to dissipate subgrid-scale energy without significantly affecting the scales resolved accurately.[24] This LES approach was developed not to artificially decrease the effective flow Reynolds number, which might be the case using eddy-viscosity subgrid models.[25] More details on this approach based on relaxation filtering, which can be referred to as LES-RF, are available in a recent paper.[26] Finally, in order to compute the radiated noise directly, non-reflective boundary conditions[27,28] are specified, with the addition of a sponge zone at the outflow.

The main parameters of the LES grids, as well as the numbers of time steps and the non-dimensional simulation times Tu_j/D of the different simulations, are provided in table 2. The grids contain from 22 to 48 millions of points, and are characterized by the radial and axial mesh spacings Δr and Δz shown in figure 1. The mesh grids are adjusted to the varying exit boundary-layer thicknesses by specifying minimum mesh spacings at the nozzle lip $\Delta r = \delta/7$ and $\Delta z = 2\delta/7$, yielding $\Delta r = 0.028r_0$ in JetD02 down to $\Delta r = 0.0035r_0$

in JetD0025. They are then stretched at rates lower than 4% to reach maximum values $\Delta r = \Delta z = 0.056 r_0$ in the physical computational domains. This mesh size is chosen so that the time frequency f of waves discretized by four grid points corresponds to Strouhal number $\mathrm{St} = fD/u_j = 10$. Grid stretching enables in particular to avoid excessive numbers of grid points in the pipe. There are for example only 154 points within the pipe diameter in JetD0025, which is still affordable compared to the 560 points that would be required using an uniform grid. Finally the grids extend radially up to $r \simeq 8.6 r_0$, and the sponge zones are built from the axial position $z = 25.5 r_0$.

Table 2. Numbers of grid points (n_r, n_θ, n_z), of points within the pipe n_r^{pipe} and n_z^{pipe}, mesh spacings at the pipe lip, number of time steps n_t, and simulation time T. The parameters for JetD005p250 and JetD005p2000 are the same as those for JetD005.

Reference	$n_r \times n_\theta \times n_z$	n_r^{pipe}	n_z^{pipe}	$\Delta r(r = r_0)$	$\Delta z(z = 0)$	n_t	Tu_j/D
JetD02	$173 \times 256 \times 505$	70	20	$0.028 r_0$	$0.056 r_0$	48,800	275
JetD01	$215 \times 256 \times 543$	94	27	$0.014 r_0$	$0.028 r_0$	46,800	275
JetD005	$249 \times 256 \times 595$	124	35	$0.007 r_0$	$0.014 r_0$	86,000	250
JetD0025	$287 \times 256 \times 651$	154	44	$0.0035 r_0$	$0.007 r_0$	127,800	187.5

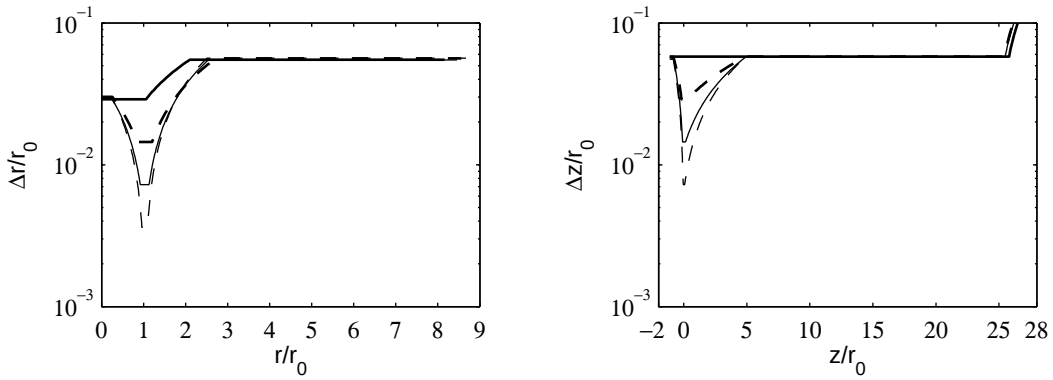

Figure 1. Mesh spacings in the radial and axial directions, Δr and Δz, in the LES, for: ——— JetD02, – – – JetD01, ——— JetD005, – – – JetD0025, ——— JetD005p250, – – – JetD005p2000.

For the study of jet turbulence features and the far-field acoustic extrapolation, density, velocity components and pressure are recorded from time $t = 37.5D/u_j$ at every points along the centerline at $r = 0$, and on cylindrical surfaces located at $r = r_0$ and at $r = 5.25 r_0$, at a frequency allowing computation of spectra up to Strouhal number 10. The velocity spectra are moreover evaluated from overlapping samples of duration $10D/u_j$. The flow statistics are also determined from $t = 87.5D/u_j$, and results are averaged in the azimuthal direction.

C. Nozzle-exit conditions

The flow conditions obtained at the nozzle-pipe exit in the jet LES are presented. They are first illustrated in figure 2 with the mean and rms turbulent profiles calculated for the axial velocity at $z = 0$. The profiles of mean velocity $< u_z >$ agree with the Blasius boundary-layer profiles specified at the pipe inlet, while the fluctuation intensities are of amplitude lower than 2%. The momentum thicknesses δ_θ determined from $< u_z >$ at $z = 0$ at the exit plane are provided in table 3. They range from $0.0025 r_0$ for JetD0025 to $0.0232 r_0$ for JetD02. As for the rms levels of fluctuating velocity u'_z, maximum values near the wall are around $0.003 u_j$ for all jets except for JetD005p2000, in which the peak is about $0.02 u_j$. Therefore, following Zaman,[7,8] the initial boundary layers of the jets are fully laminar for the four jets without inlet noise and for JetD005p250, and nominally laminar for JetD005p2000. In all jets, the velocity fluctuations on the centerline are also observed to be of low amplitude, between 0.2% and 0.6% of the jet velocity. To finally compare with some experiments of the literature dealing with jet noise, it can be noted that Zaman[7,8] and Bridges and Hussain[9] measured in jets at Reynolds numbers $\mathrm{Re}_D = 10^5$ and $\mathrm{Re}_D = 1.4 \times 10^5$, respectively, initial momentum thicknesses of $\delta_\theta = 0.006 r_0$ and $\delta_\theta = 0.005 r_0$, and turbulent intensities around 0.5%. These conditions are

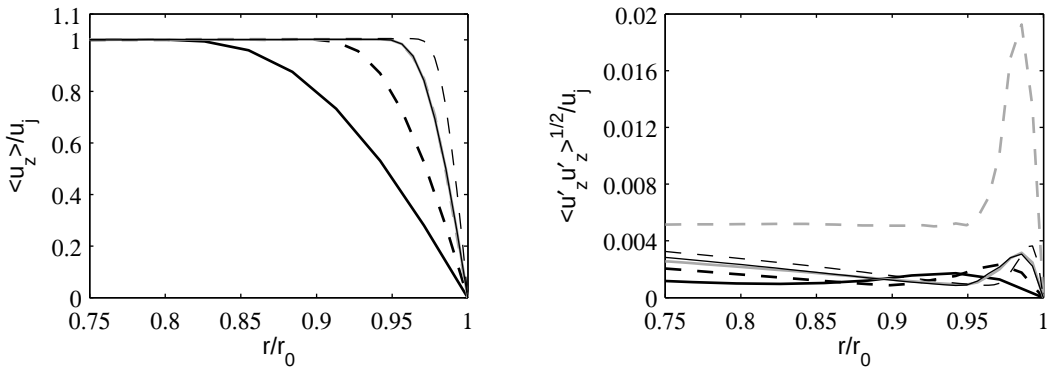

Figure 2. Profiles at $z = 0$ of mean axial velocity $< u_z >$, and of the rms values of fluctuating axial velocity u'_z, for: ——— JetD02, – – – JetD01, ——— JetD005, – – – JetD0025, ——— JetD005p250, – – – JetD005p2000.

Table 3. Shear-layer momentum thickness δ_θ at $z = 0$, and at $z = 0.4r_0$, except, (*), at $z = 0.1r_0$, centerline and maximum near-wall rms values of axial fluctuating velocity u'_z at the pipe exit at $z = 0$, and integral length scales in the azimuthal direction $L_{11}^{(\theta)}$ calculated from u'_z along the lip line at $r = r_0$, in radians.

Reference	δ_θ/r_0 at z=0	δ_θ/r_0 at z=0.4r_0	$<u_z'^2>^{1/2}/u_j$ at z=r=0	$\max(<u_z'^2>^{1/2})/u_j$ at z=0 near r=r_0	$L_{11}^{(\theta)}/\pi$ at z=0.1r_0	$\max(L_{11}^{(\theta)})/\pi$ at r=r_0
JetD02	0.0232	0.0246	0.0026	0.0017	0.59	0.79
JetD01	0.0116	0.0128	0.0054	0.0023	0.61	0.65
JetD005	0.0056	0.0072	0.0059	0.0031	0.53	0.59
JetD0025	0.0025	0.0048	0.0048	0.0036	0.40	0.44
JetD005p250	0.0056	0.0072	0.0041	0.0032	0.39	0.41
JetD005p2000	0.0056	0.0060(*)	0.0045	0.0192	0.06	0.06

quite similar to those in JetD005 and JetD005p250.

To further characterize the flow just downstream of the nozzle lip, the variations of the shear-layer momentum thickness δ_θ and of the integral length scale $L_{11}^{(\theta)}$ of fluctuating axial velocity u'_z in the azimuthal direction are presented in figure 3 for $0 \leq z \leq 2r_0$. The momentum thickness is estimated from the mean axial velocity $< u_z >$ as

$$\delta_\theta = \int_0^{r_{0.04}} \frac{< u_z >}{u_c} \left(1 - \frac{< u_z >}{u_c}\right) dr$$

where $u_c =< u_z > (r = 0)$ is the centerline mean axial velocity, and $r_{0.04}$ is determined so that $< u_z > (r = r_{0.04}) = 0.04u_c$. The azimuthal integral length scale is evaluated as

$$L_{11}^{(\theta)} = \frac{1}{r_0} \int_0^\pi \mathcal{R}_{11}^{(\theta)} d(r_0 \delta\theta)$$

from the cross-correlation function $\mathcal{R}_{11}^{(\theta)}$ of velocity u'_z defined by

$$\mathcal{R}_{11}^{(\theta)}(r, \delta\theta, z) = \frac{\langle u'_z(r, \theta, z) u'_z(r, \theta + \delta\theta, z) \rangle}{\langle u'^2_z(r, \theta, z) \rangle^{1/2} \langle u'^2_z(r, \theta + \delta\theta, z) \rangle^{1/2}}$$

where $\delta\theta$ is the azimuthal separation, and $\langle . \rangle$ denotes statistical averaging. The length scale, calculated at $r = r0$, is normalized by r_0 to be in radians. For the axisymmetric mode, $L_{11}^{(\theta)} = \pi$ would for instance be obtained.

The variations of δ_θ in figure 3 display two distinct stages typical of the development of initially laminar shear layers.[4–6] The momentum thickness first grows slowly during the flow adjustment following the nozzle lip, from a boundary-layer velocity profile to a shear-layer velocity profile, then increases rapidly when vortical structures appear, as evidenced by the snapshots of figure 7. This second stage of shear-layer

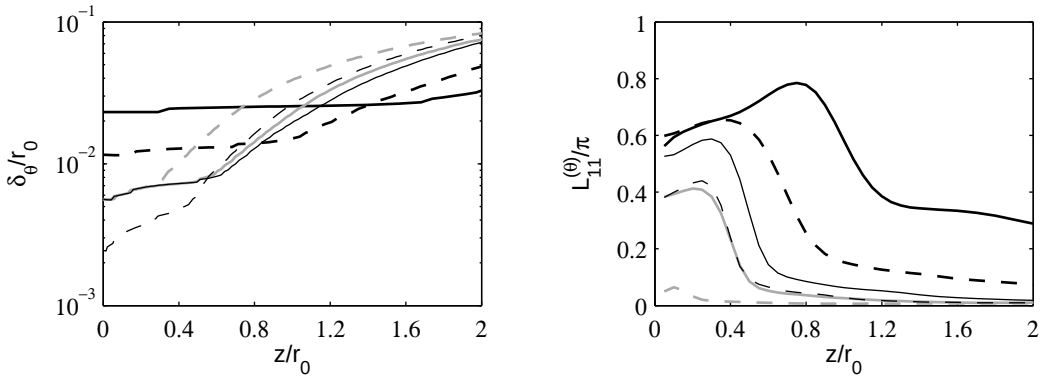

Figure 3. Axial variations in the vicinity of the pipe lip, of the shear-layer momentum thickness δ_θ, and of the integral length scale in the azimuthal direction $L_{11}^{(\theta)}$ calculated from the fluctuating axial velocity at $r = r_0$, for: ——— JetD02, – – – JetD01, ——— JetD005, – – – JetD0025, ——— JetD005p250, – – – JetD005p2000.

development takes place earlier when the nozzle-exit δ_θ is smaller, in agreement with the linear instability theory[29] predicting that instability waves grow at higher rates for sharper velocity gradients, and when inlet noise is introduced. Moreover, during the first stage, the laminar shear layer spreads in a negligible manner in JetD02, but more significantly as the initial momentum thickness becomes smaller, which is certainly due to molecular viscosity. Therefore, given the appreciable variations of δ_θ during the early transition, the values of momentum thickness which will be used later as the initial shear-layer thickness are taken at $z = 0.1r_0$ for JetD005p2000, and at $z = 0.4r_0$ for all other jets. They are provided in table 3.

The azimuthal integral length scales $L_{11}^{(\theta)}$ at $r = r_0$ exhibit similar axial variations in figure 3, with a slight increase just downstream of the exit plane, rapidly followed by a collapse down to much smaller values. Peak and initial values at $z = 0.1r_0$ are reported in table 3. In the vicinity of the nozzle exit, length scales up to 0.59π are noticed, which indicates that azimuthal correlation is high in the present laminar shear layers. The addition of random pressure disturbances in the pipe however appears to lower the initial azimuthal correlations: from $L_{11}^{(\theta)} = 0.53\pi$ for JetD005, one gets $L_{11}^{(\theta)} = 0.39\pi$ for JetD005p250, and only $L_{11}^{(\theta)} = 0.06\pi$ for JetD005p2000. At this point it can be worth pointing out that the nozzle-exit conditions in JetD005 and JetD005p250 are very close: mean velocity profiles and turbulent intensities are the same, whereas the azimuthal velocity correlations differ.

D. Far-field extrapolation

For the characterization of the noise generated by the jets, and the comparison with experimental data, the near field obtained directly by LES is propagated in the acoustic far field. The sound propagation is carried out by solving the linear acoustic equations written in cylindrical coordinates, for the fluctuating velocity components and pressure as in previous works.[30,31] The numerical schemes and boundary conditions used are the same as those implemented in the LES. The non-centered finite differences and filters developed by Berland *et al.*[23] are in particular applied at the inner-side boundary of the extrapolation grid where the LES data are introduced.

In practice, the far-field extrapolation is performed from the velocity components and pressure recorded in the LES from time $t = 37.5D/u_j$ at every point at $r = 5.25r_0$, at a frequency allowing computation of spectra up to Strouhal number 10. These data are interpolated on a cylindrical surface discretized by a uniform mesh spacing $\Delta z = 0.056r_0$ in the axial direction, thus containing 450 points from $z = -0.6r_0$ to $z = 25r_0$. They are then imposed at the bottom boundary of a cylindrical grid of $n_r \times n_\theta \times n_z = 751 \times 256 \times 881$ points, extending up to $z = 54r_0$ and $r = 61.5r_0$, on which the linear acoustic equations are solved to propagate noise. The mesh spacings of the extrapolation grid are shown in figure 4. The maximum mesh size is $\Delta r = \Delta z = 0.075r_0$, yielding Strouhal number St = 7.4 for the sound waves discretized by four grid points. After a propagation time $t = 30D/u_j$, pressure is recorded around the jets at points located at $60r_0$ from $z = r = 0$, during time periods of $225D/u_j$ for JetD02 and JetD01, $200D/u_j$ for JetD005, JetD005p250 and JetD005p2000, and $135D/u_j$ for JetD0025. Spectra are evaluated from the pressure signals using overlapping samples of duration $30D/u_j$, and they are also averaged in the azimuthal direction.

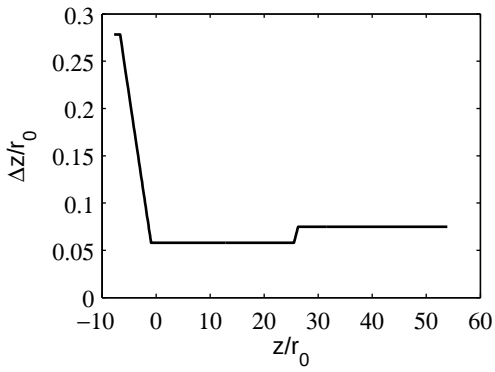

Figure 4. Mesh spacing in the axial direction Δz in the acoustical simulations. The mesh spacing in the radial direction is $\Delta r = 0.075 r_0$.

E. Corresponding experiments

The simulation results will be compared in the next section with measurements. For the aerodynamic fields, the data obtained by Hussain and Zedan,[4] and Husain and Hussain[6] in axisymmetric mixing layers, and by Lau *et al.*,[32] Arakeri *et al.*[33] and Fleury *et al.*[34] in round jets at Mach number 0.9 and Reynolds numbers higher than 5×10^5 will be used. In the same way, for the acoustic fields, the sound pressure levels and spectra provided by Zaman[7,8] for initially laminar jets, and by Mollo-Christensen *et al.*,[35] Lush,[36] Tanna[37] and Bogey *et al.*[38] for jets at $\mathrm{M} \simeq 0.9$ and $\mathrm{Re}_D \geq 5 \times 10^5$ will be considered. Some available parameters of these experiments are documented in table 4.

Table 4. Jet experiments: Mach and Reynolds numbers M and Re_D, initial shear-layer momentum thickness δ_θ, maximum intensity of fluctuating velocity u'_z at the nozzle exit, and symbols used in the plots. The arrow indicates the variations in a set of experiments.

Reference	M	$\mathrm{Re}_D \times 10^{-5}$	$\delta_\theta / r_0 \times 10^3$	u'_z/u_j	Symbols
Hussain and Zedan[4]	$0.038 \rightarrow 0.075$	$0.66 \rightarrow 1.3$	$9.2 \rightarrow 2.8$	0.06	$\triangledown$
Husain and Hussain[6]	0.09	2.5	3.3	0.025	$\triangle$
Lau *et al.*[32]	0.9	10	-	-	$\circ$
Arakeri *et al.*[33]	0.9	5	50	0.10	$\square$
Fleury *et al.*[34]	0.9	7.7	-	-	$\diamond$
Zaman[7,8]	$0.12 \rightarrow 0.43$	$0.7 \rightarrow 2.5$	$7.9 \rightarrow 4.6$	$0 \rightarrow 0.10$	-
Mollo-Christensen *et al.*[35]	0.9	5.4	-	-	$+$
Lush[36]	0.88	5	-	-	$\times$
Tanna[37]	0.9	10	-	-	$\triangleleft$
Bogey *et al.*[38]	0.9	7.8	-	-	$\triangleright$

The initial momentum thicknesses of the axisymmetric mixing layers investigated by Hussain and Zedan[4] and Husain and Hussain[6] are similar to those specified in JetD005, JetD005p250 and JetD005p2000, and in JetD0025, which are $\delta_\theta = 0.056 r_0$ and $\delta_\theta = 0.025 r_0$, respectively, see in table 3. The inflow turbulent intensities are however higher with respect to the simulations, except for JetD005p2000 in which the peak rms axial fluctuating velocity is around 2% of the jet velocity as in Hussain and Zedan.[4] Regarding the seven jets[32–38] at Mach numbers around 0.9, they can be assumed to be initially turbulent because their high Reynolds numbers.

Finally some experimental results obtained by Zaman[7,8] are presented in figure 5. The variations of the momentum thickness and maximum turbulent intensity at the nozzle exit in untripped jets at $\mathrm{Re}_D \leq 2.5 \times 10^5$ are first illustrated. The decrease of δ_θ / r_0 and the growth of u'_z/u_j with the Reynolds number are clearly shown. The sound spectra measured at an angle of 90° for untripped (laminar) jets are also compared with that obtained for a tripped (turbulent) jet. They are characterized by additional high-frequency peaks, attributed by Zaman[7,8] to the first stage of pairing of the shear-layer coherent vortices.

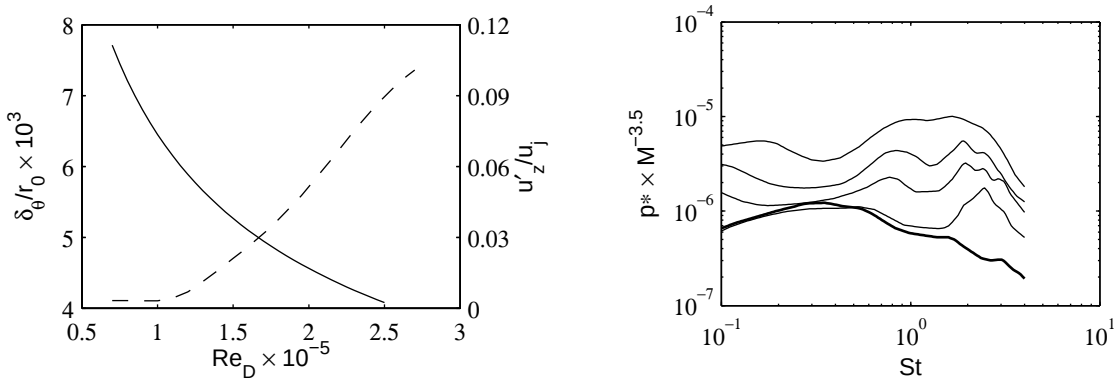

Figure 5. Experimental results by Zaman.[7,8] Left: variations of nozzle-exit, ——— boundary-layer momentum thickness δ_θ and – – – maximum turbulent intensity u'_z/u_j, with Reynolds number Re_D for untripped jets. Right: far-field pressure spectra at 90° for, ——— untripped jets at $Re_D = 0.7 \times 10^5$, 0.8×10^5, 10^5 and 1.3×10^5 (from top to bottom) and ——— a tripped jet at $Re_D = 1.3 \times 10^5$.

III. Simulation results

The effects of the jet initial conditions are presented in this section by showing vorticity and sound pressure snapshots, and the main characteristics of the mean and turbulent developments of the shear layers and jet flows, as well as of the features of the acoustic fields. When possible, the simulation results are compared to the data provided by the experiments reported in section II.E.

A. Vorticity and pressure snapshots

Snapshots of vorticity norm obtained for the present jets are displayed in figure 6. In the initially laminar shear layers, the turbulent transition first seems to be dominated by coherent structures, then three-dimensional fine-scale turbulence is generated. Farther downstream the mixing layers merge and turbulent jets are observed. From these overall jet pictures, it is difficult to clearly see the differences between the jet developments. Some effect of the nozzle-exit boundary-layer thickness are however visible, by comparing for instance the vorticity fields in JetD02 and JetD0025. For smaller initial δ_θ, vortical structures appear to form more rapidly in the shear layers. The mixing layers, once turbulent, also develop more slowly, leading to an increase of the potential core length, around $10r_0$ in JetD02 versus $18r_0$ in JetD0025.

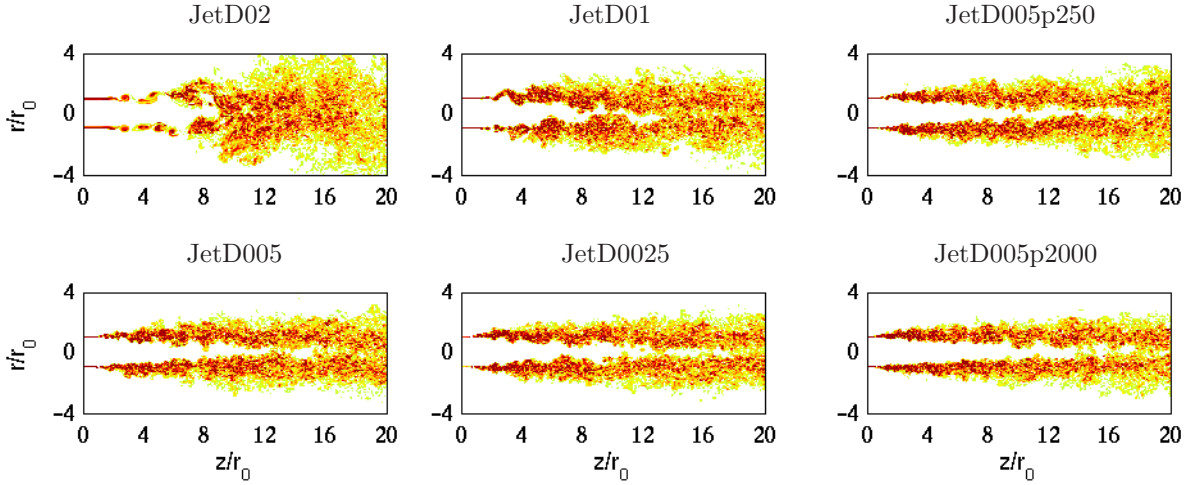

Figure 6. Snapshots in the (z, r) plane of vorticity norm. The color scale ranges up to the level of $6.5u_j/r_0$.

To focus on the early jet flow development, vorticity snapshots obtained in the shear layers close to the exit plane are represented in figure 7. In the four jets without inlet noise, JetD02, JetD01, JetD005 and JetD0025, the mechanisms taking place downstream of the nozzle lip are the same. The turbulent transition

in the initially laminar mixing layers first consists of the processes of vortex rolling-up and pairing, whatever the exit boundary-layer thickness, then 3-D turbulence appears after the first vortex pairing. The variations of the initial momentum thickness is found to affect the size of the coherent structures generated by the shear-layer rolling-up. As δ_θ decreases, these structures are significantly smaller, as expected. The rolling-up also occurs farther upstream. Finally the vorticity fields obtained for JetD005p250 and JetD005p2000 are fairly similar to that for JetD005, with same δ_θ at $z = 0$. In the two former jets, however, the mixing layers develop earlier while exhibiting less organized vortical structures. This suggests that the rolling-up/pairing process is hindered by the addition of low random noise inside the pipe.

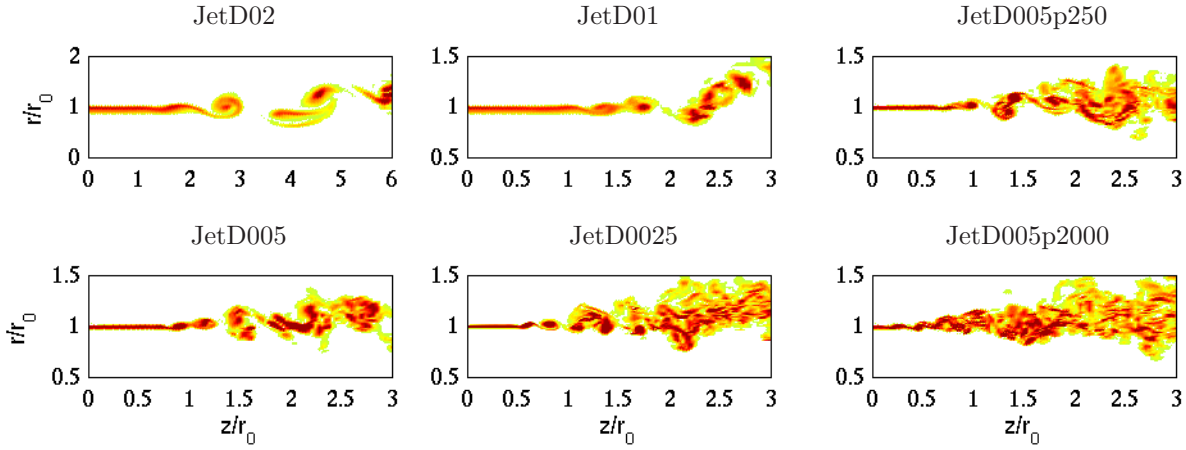

Figure 7. Snapshots in the (z, r) plane of vorticity norm downstream of the pipe lip. The color scale ranges up to the level of $10u_j/r_0$ for JetD02, but up to $20u_j/r_0$ for the other jets.

As first illustrations of the noise generated by the jets, snapshots of the near pressure fields determined directly by LES are shown in figure 8. In JetD02, JetD01, JetD005 and JetD0025, strong acoustic waves are seen to propagate at wide angles, typically between 60° and 90°, relative to the jet direction. These waves visibly come from the transition region of the shear layers. Their apparent origins, which are closer to the jet exit as the initial shear-layer thickness decreases, even correspond roughly to the locations of the first vortex pairing in the mixing layers. Additionally, their associated wavelengths and levels are found both to be significantly reduced when smaller δ_θ is specified at the nozzle exit. Concerning the near pressure fields obtained for JetD005p250 and JetD005p2000, they display features similar as that for JetD005. The acoustic waves radiated by these two jets are however of lower amplitude.

The near acoustic fields issued from the LES are propagated at 60 radii from the nozzle exit, by solving the linear acoustical equations as described in section II.D. The wave extrapolation is performed from a cylindrical control surface located at $r = 5.25r_0$, extending from $z = -0.6r_0$ to $z = 25r_0$ in the axial direction. A snapshot of the pressure field thus determined for JetD005p2000 is presented in figure 9. The propagation of the sound waves generated in the turbulent shear layers seems to be properly taken into account. Unfortunately low-frequency waves of high magnitude originating from the end of the control surface are also observed. The presence of these spurious waves is not fully understood at the present time, but it can reasonably be assumed that in its downstream part the control surface is too close to the aerodynamic flow field. This led us to carry out additional far-field extrapolations using control surfaces limited to $z \leq z_c + 2r_0$ in the axial direction, where z_c is the axial location of the end of the potential core given later in table 6. In this way, as shown in figure 9, the low-frequency unphysical waves are weakened without appreciably affecting the waves emitted by the jets in the sideline direction. The latter point is in particular supported by pressure spectra. The sound spectra which will be presented in section III.D. for radiation angles of 60° and 90° are therefore estimated using these shortened surfaces, the other sound field features being obtained from the full control surface.

B. Shear-layer development

The growth of the shear layer in the different jets is first investigated by displaying in figure 10 the variations of the momentum thickness δ_θ and of the spreading rate $\mathrm{d}\delta_\theta/\mathrm{d}z$ for $z \leq 8r_0$. As the initial momentum thickness becomes smaller, according to the graphs of δ_θ, the shear layers develop earlier, but more slowly. This

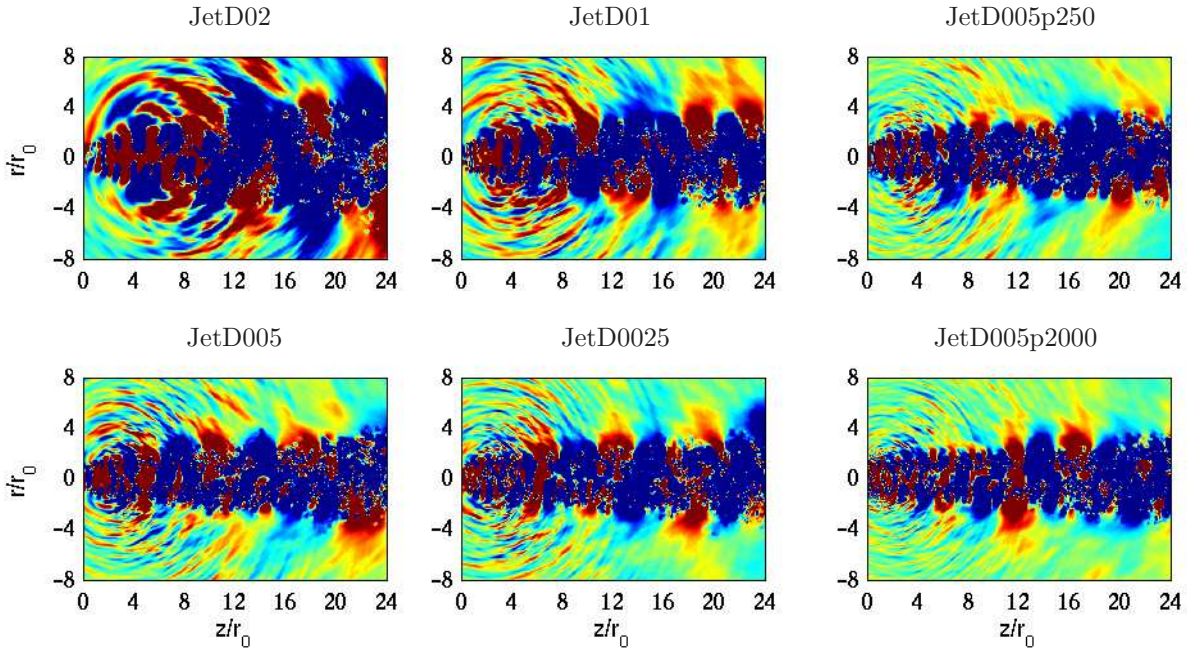

Figure 8. Snapshots in the (z, r) plane of the fluctuating pressure obtained by LES. The color scale ranges for levels from -250 to 250 Pa.

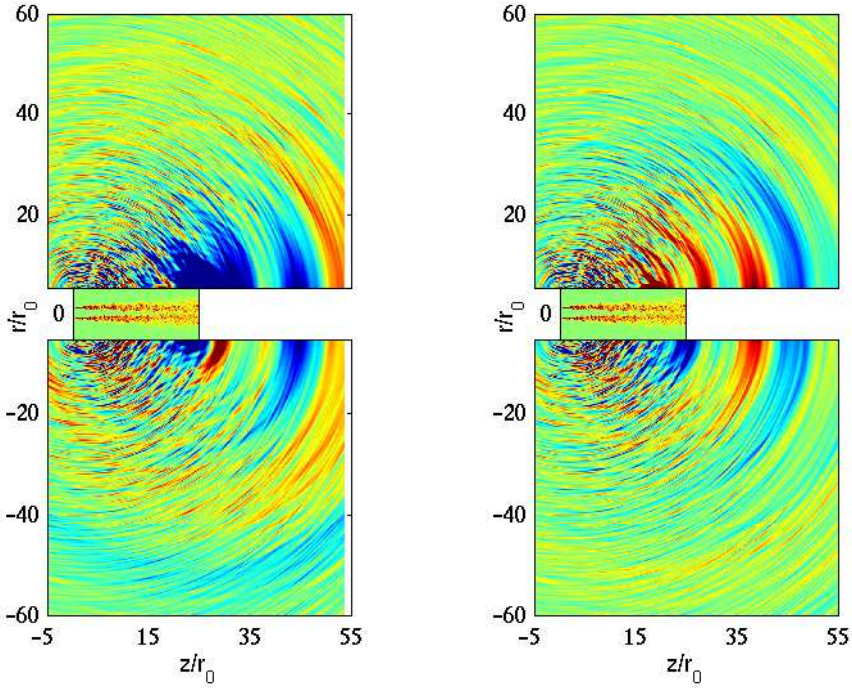

Figure 9. Snapshots in the (z, r) plane of the pressure field obtained from the acoustical simulations for JetD005p2000, using the full control surface (left) and a control surface limited to $z \leq z_c + 2r_0$ (right), where z_c is the position of the potential core end. The color scales range from -40 to 40 Pa for pressure, and up to $8u_j/r_0$ for vorticity norm in the LES jet flow.

observation is supported quantitatively by the spreading rates, which reach peaks more rapidly, but display high values over shorter axial distance for thinner shear layer. This behaviour is moreover strengthened by the addition of inlet random noise inside the nozzle.

Experimental data provided by Hussain and Zedan,[4] and by Husain and Hussain[6] for axisymmetric initially laminar mixing layers are also represented in figure 10. The agreement with the LES results is poor for JetD02 and JetD01, but rather satisfactory for the other jets with exit boundary layers so that $\delta_\theta \leq 0.0056 r_0$ at $z = 0$. The variations of the spreading rate $\mathrm{d}\delta_\theta/\mathrm{d}z$ given by Hussain and Zedan[4] in particular best compare with those obtained for JetD005p2000. This could be expected because of the experimental initial parameters collected in table 4. The mixing layer of Husain and Hussain[6] was indeed characterized at the exit plane by a thickness $\delta_\theta = 0.003 r_0$, and by axial turbulent intensities around 2% as in JetD005p2000. For similar inflow conditions, simulations and experiments thus appear to yield close solutions.

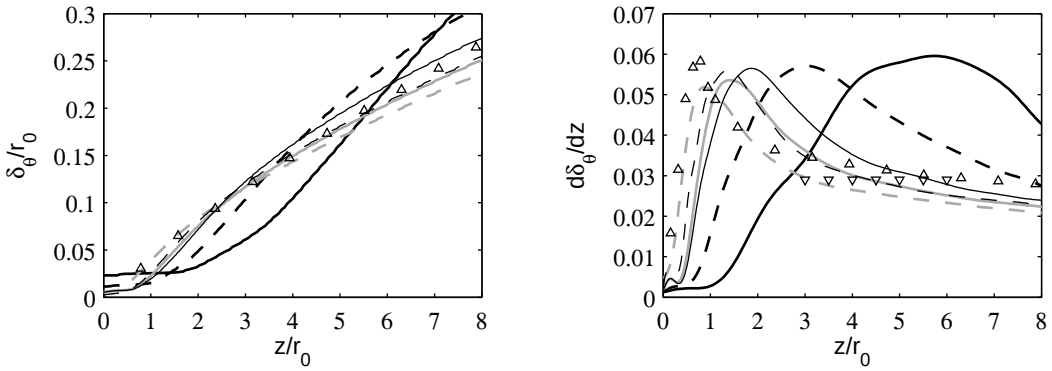

Figure 10. Variations of shear-layer momentum thickness δ_θ, and of spreading rate $\mathrm{d}\delta_\theta/\mathrm{d}z$, for: ——— JetD02, – – – JetD01, ——— JetD005, – – – JetD0025, ——— JetD005p250, – – – JetD005p2000. Measurements: ▽ Hussain and Zedan,[4] △ Husain and Hussain.[6]

The intensities of turbulence in the shear layers are shown in figure 11 with the variations of the levels of fluctuating axial, radial and azimuthal velocities, and of the Reynolds stress along the lip line. In agreement with previous results, they grow more rapidly in thinner shear layers, and when random noise is introduced upstream. For all components except azimuthal velocity u'_θ, the curves obtained for the jets without inlet noise, JetD02, JetD01, JetD005 and JetD0025, exhibit dual-peak shapes, which is typical, from Zaman and Hussain,[39] of the presence of strong vortex pairings at a fixed location. This feature is however not observed for JetD005p250 and JetD005p2000. It is also interesting to notice that the peak levels obtained for velocity u'_z are all around $0.23 u_j$, whereas the peak levels for velocity u'_r are around $0.22 u_j$ for JetD02, JetD01, JetD005 and JetD0025, but decrease down to $0.18 u_j$ for JetD005p2000, as reported in table 6. These results give evidence of the significant changes that occur in the shear-layer turbulence when transition is initially affected by random disturbances even of very low magnitude, the rolling-up/pairing process being of less importance in this case. This sensitivity to inflow disturbances may have weak influence on the jet flow development, but notable consequences on the acoustic field, which will be shown in section III.D.

Table 5. Positions z_{roll} and z_{pair} at which velocity spectra are calculated along the lip line at $r = r_0$, peak Strouhal number in radial velocity spectra at $r = r_0$ and $z = z_{pair}$, and peak rms values of axial and radial fluctuating velocities u'_z and u'_r along the lip line.

Reference	z_{roll}/r_0	z_{pair}/r_0	St^{peak}_{pair}	$<u'^2_z>^{1/2}/u_j$ max at r=r_0	$<u'^2_r>^{1/2}/u_j$ max at r=r_0
JetD02	2.5	4.8	0.54	0.233	0.226
JetD01	1.7	2.6	0.96	0.225	0.223
JetD005	1.1	1.6	1.61	0.223	0.222
JetD0025	0.8	1.2	2.48	0.224	0.222
JetD005p250	0.95	1.3	1.88	0.219	0.201
JetD005p2000	0.6	0.9	2.16	0.215	0.181

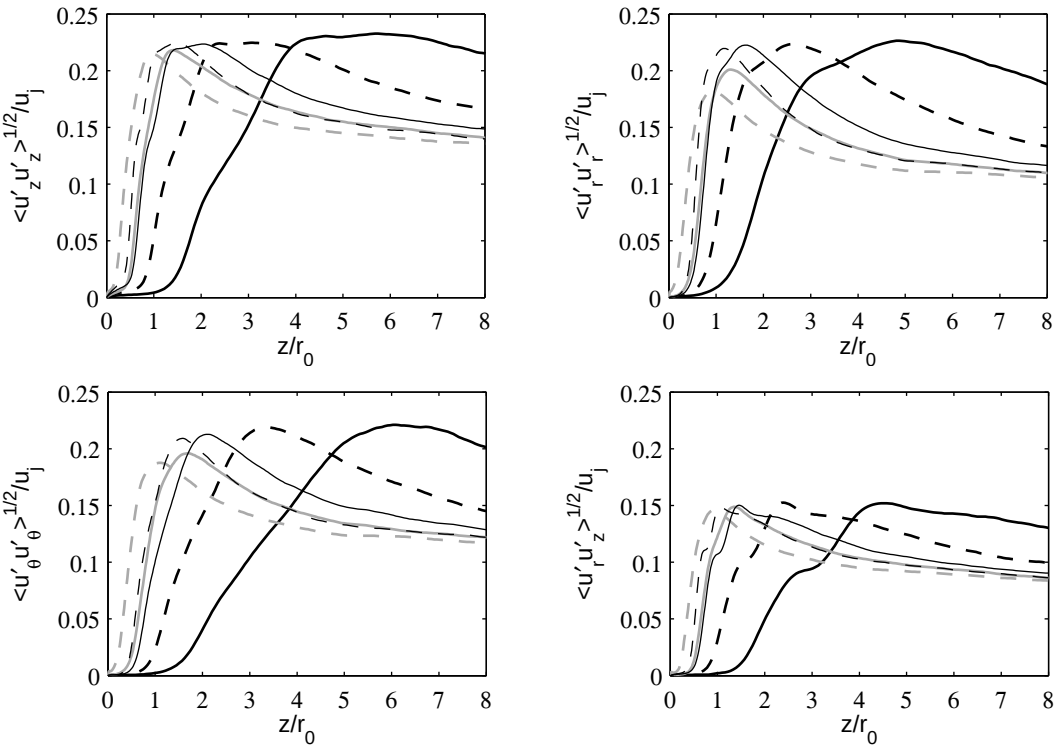

Figure 11. Variations along the lip line at $r = r_0$ of the rms values of fluctuating velocities u'_z, u'_r and u'_θ, and of the magnitude of Reynolds stress $< u'_r u'_z >$, for: ——— JetD02, – – – JetD01, ——— JetD005, – – – JetD0025, ——— JetD005p250, – – – JetD005p2000.

Spectra of the fluctuating radial velocity u'_r obtained along the lip line are finally presented in figure 12. They are computed at two positions z_{roll} and z_{pair} given in table 5, corresponding approximately to the location of the vortex rolling-up and to the end of the first pairing, respectively. More precisely, z_{pair} is taken at the peak of the rms fluctuating velocity u'_r along $r = r_0$, and z_{roll} is near the inflection point that is observed in the graphs of the Reynolds stress $< u'_r u'_z >$ in figure 11, when possible. Arrows are also plotted in figure 12 to show the frequencies evaluated in the jets from the momentum thickness found slightly downstream of the exit section, provided in the second column of table 3, using the formula $f\delta_\theta/u_j = 0.012$. In left figure, at $z = z_{roll}$, the velocity spectra are dominated by peaks at Strouhal numbers $\mathrm{St} = fD/u_j$ very close to the values indicated by the arrows. The rollings-up therefore develop at frequencies in agreement with those found experimentally in initially laminar mixing layers, as in the works of Zaman[7,8] for instance. In right figure, at $z = z_{pair}$, the velocity spectra exhibit peaks at Strouhal numbers St^{peak}_{pair}, reported in table 5, which are the first subharmonics of the rolling-up frequencies. This behaviour is observed in all jets. Nevertheless it is less pronounced in jets with thinner initial shear layers, and when inlet random noise is introduced inside the pipe nozzle, which implies that the rolling-up/pairing process is then weaker.

C. Jet flow development

The effects of the nozzle-exit conditions on the mean flow field of the circular jets are shown in figure 13 with the profiles of centerline mean axial velocity $u_c =< u_z > (r = 0)$ and of the jet half-width $\delta_{0.5}$ defined by $< u_z > (r = \delta_{0.5}) = u_c/2$. When the initial momentum thickness δ_θ is reduced, as suggested by previous results, the jets start to develop on the centerline, and to spread radially, at farther axial distances. This results in longer potential cores, in agreement with the simulations of Kim and Choi[13] for a jet at $\mathrm{Re}_D = 10^5$. To quantify the core elongation, the positions z_c of the end of the potential core in the present jets are given in table 6. They are here evaluated using $u_c(z = z_c) = 0.95u_j$. For the four jets without inlet noise, they range from $z_c = 8.6r_0$ for JetD02 up to $z_c = 16.8r_0$ for JetD0025. The values obtained for JetD005p250 and JetD005p2000 are also $z_c = 16.4r_0$ and $z_c = 18.1r_0$, respectively. They are larger than the value $z_c = 14.1r_0$ found for JetD005, which indicates that the potential core length increases with the magnitude of the inlet

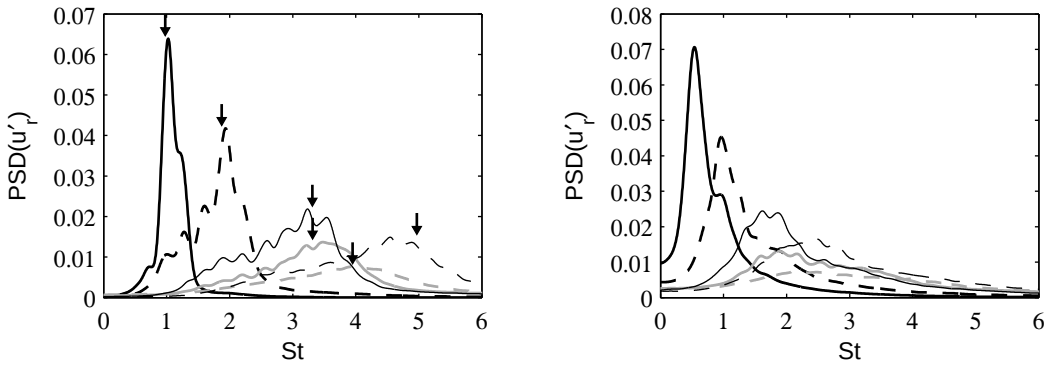

Figure 12. Spectra of velocity u'_r obtained at $r = r_0$, as functions of Strouhal number $\mathrm{St} = fD/u_j$. Left, around rolling-up at $z = z_{roll}$, right, just downstream of pairing at $z = z_{pair}$, for: ——— JetD02, – – – JetD01, ——— JetD005, – – – JetD0025, ——— JetD005p250, – – – JetD005p2000 (z_{roll} and z_{pair} are given in table 5). The arrows indicate the frequencies determined from the initial momentum thickness using $f\delta_\theta/u_j = 0.012$.

random disturbances. The jet mean flow therefore develops more slowly when the exit δ_θ becomes smaller, or when random noise is added in the pipe.

For comparison with experimental data, the centerline velocity decays and jet spreadings obtained by Lau *et al.*,[32] Arakeri *et al.*[33] and Fleury *et al.*[34] for Mach 0.9 jets at Reynolds numbers $\mathrm{Re}_D \geq 5 \times 10^5$ are depicted in figure 13. Despite uncertainties and possible variations in the experimental initial conditions, the jet of Arakeri *et al.*[33] being for instance characterized by $\delta_\theta = 0.05r_0$ and rms values of u'_z around 10% u_j at the nozzle exit (refer to table 4), the measurements are rather close. This probably results from the fact that at such Reynolds numbers the jets are certainly all initially turbulent. For both u_c and $\delta_{0.5}$, the experimental data fairly agree with the curves determined for the jets simulated with thin initial shear layers. They fall in particular especially well on the profiles for JetD005 in which $\delta_\theta = 0.006r_0$ at $z = 0$.

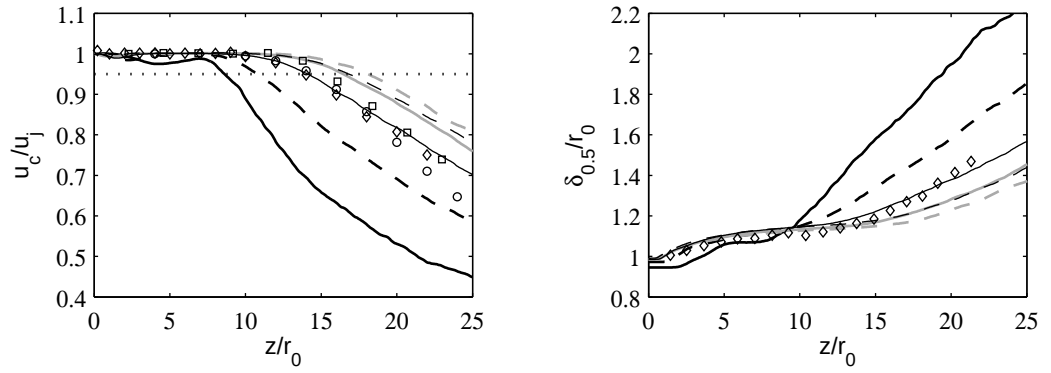

Figure 13. Variations of centerline mean axial velocity u_c and of jet half-width $\delta_{0.5}$, for: ——— JetD02, – – – JetD01, ——— JetD005, – – – JetD0025, ——— JetD005p250, – – – JetD005p2000 (the dotted line represents $u_c = 0.95u_j$). Measurements: ○ Lau *et al.*,[32] □ Arakeri *et al.*,[33] ◇ Fleury *et al.*[34]

To characterize the magnitude of the jet turbulence, the levels of the fluctuating axial and radial velocities along the centerline are presented in figure 14. As the initial shear-layer thickness decreases, they reach peaks with lower amplitude, farther in the downstream direction, both for the axial velocity u'_z as in Kim and Choi,[13] and for the radial velocity u'_r. In table 6, the maxima of the centerline rms levels for u'_r are for instance reported to be $0.134u_j$ for JetD02, but only $0.057u_j$ for JetD0025. This trend could be due to the apparently contradictory results of getting earlier shear-layer development but also longer potential core when δ_θ becomes smaller at the nozzle exit. The shear-layer transition, and consequently its related high rms velocity levels around $0.2u_j$ observed in figure 11, thus occur farther from the end of the potential core where the shear-layer vortical structures merge on the jet axis, which leads to lower centerline turbulence intensities. Regarding the influence of adding inflow noise, it appears minor because the peaks of the fluctuation levels for JetD005p250 and JetD005p2000 are very similar to those for JetD005 with same initial δ_θ.

Table 6. Axial position of the end of the potential core z_c, and peak rms values of axial and radial fluctuating velocities u'_z and u'_r along the centerline.

Reference	z_c/r_0	$<u'^2_z>^{1/2}/u_j$ max at r=0	$<u'^2_r>^{1/2}/u_j$ max at r=0
JetD02	8.6	0.164	0.139
JetD01	10.8	0.124	0.093
JetD005	14.1	0.109	0.071
JetD0025	16.8	0.105	0.057
JetD005p250	16.4	0.104	0.071
JetD005p2000	18.1	0.101	0.069

As previously for the mean flow features, comparisons with measurements by Lau *et al.*,[32] Arakeri *et al.*[33] and Fleury *et al.*[34] are made. Albeit significantly scattered, in particular for the radial velocity component, the experimental data are somewhat closer to the results obtained for the jets with thinner nozzle-exit boundary layer. The data from Arakeri *et al.*[33] are especially in good agreement with the rms velocity levels for JetD005.

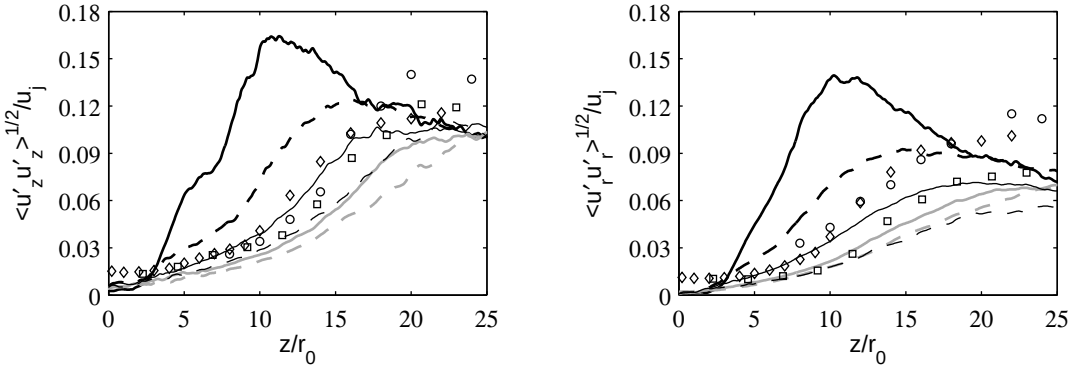

Figure 14. Variations along the centerline at $r = 0$ of the rms values of fluctuating velocities u'_z and u'_r, for: ——— JetD02, – – – JetD01, ——— JetD005, – – – JetD0025, ——— JetD005p250, – – – JetD005p2000. Measurements: ○ Lau *et al.*,[32] □ Arakeri *et al.*,[33] ◇ Fleury *et al.*[34]

D. Acoustic far field

The pressure spectra obtained at 60 radii from the pipe exit from the far-field extrapolation of the LES near fields, for radiation angles of 30°, 40°, 60° and 90° relative to the jet direction, are represented in figure 15. For all angles, parasitic low-frequency components, certainly coming from the downstream part of the control surface as discussed in section II.D., are noted for Strouhal numbers lower than 0.15. More interestingly, compared to sound spectra provided by Tanna[37] and Bogey *et al.*[38] for experimental jets at Reynolds numbers $\mathrm{Re}_D \geq 7.8 \times 10^5$ (see in table 4), the spectra contain additional high-frequency bumps. These extra noise components are especially of high magnitude for the jets simulated without inlet random disturbance. They are in addition characterized by peak frequencies in good agreement with the Strouhal numbers St^{peak}_{pair} of the first vortex pairing in the shear layers, given in table 5, and indicated by arrows in the pressure spectra for JetD02, JetD01, JetD005 and JetD0025. The present numerical results hence show the additional acoustic radiation due to vortex pairings in initially laminar jets. They are very similar to the findings of the experimental works conducted by Zaman[7,8] and by Bridges and Hussain[9] to study noise generation in tripped/untripped jets. To see that more clearly, consider for instance the great resemblance between the sound spectra determined in the sideline direction from the simulations in figure 15 and those from Zaman[7,8] in figure 5.

When the nozzle-exit boundary-layer thickness becomes smaller, the vortex pairing noise moves to higher frequencies, as expected. The low-frequency parts of the spectra then are less and less affected by the pairing noise, and consequently gets closer to the spectra obtained experimentally for high Reynolds number jets.

This behaviour is found for all radiation angles. It is for example well visible in the spectra obtained at the angle of 90° for which the sound levels from JetD005 and JetD0025 over $0.15 \leq \mathrm{St} \leq 0.4$ are close, and similar to the measurements. As the initial δ_θ is reduced in the simulations, the pairing noise levels also appear to decrease. This could be connected to the fact that in jets with thinner shear layers, as evidenced in table 3 and in figure 3, the azimuthal correlations of velocity fluctuations in the first few diameters downstream of the exit section are lower, thus leading to weaker vortex pairings and less efficient noise sources.

Finally the addition of inlet random noise inside the pipe nozzle is observed to strongly alter the far-field sound spectra, especially for large radiation angles. The bumps associated with vortex pairing noise are seen to progressively lessen. With respect to JetD005 without inlet noise, the peaks in the pressure spectra evaluated at 90° are then reduced by 5 dB in JetD005p250, and by 8 dB in JetD005p2000. The lowering of the pairing noise in the two latter jets is not surprising, because of the weakening of the rolling-up/pairing process shown in section III.B. The modifications of the acoustic fields are however quite spectacular and rather unexpected given the jet initial conditions. Compare for instance the minute differences between the nozzle-exit conditions of JetD005 and JetD005p250 (same boundary-layer momentum thicknesses and rms velocity fluctuations, but slightly lower azimuthal velocity correlations in JetD005p250, as mentioned in table 3), with the 5 dB reduction in the sideline sound spectra.

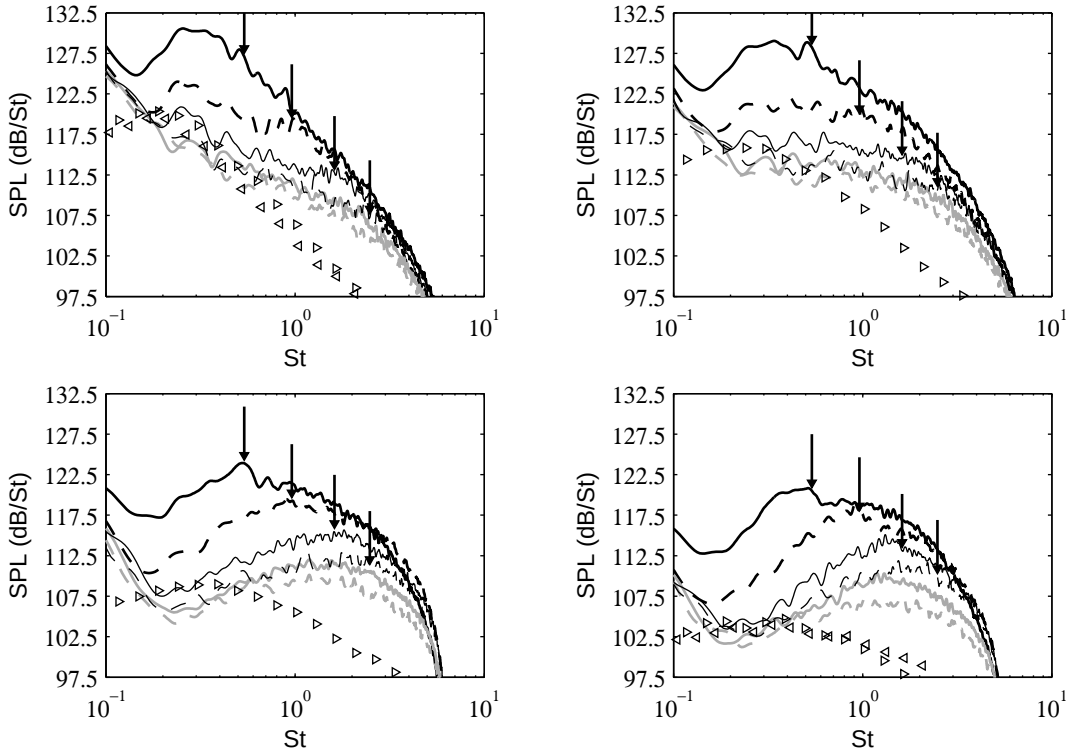

Figure 15. Sound pressure spectra obtained at $60r_0$ from the jet nozzle exit, as functions of Strouhal number $\mathrm{St} = fD/u_j$, for radiation angles relative to the jet direction of: 30° (top left), 40° (top right), 60° (bottom left), and 90° (bottom right), for: ——— JetD02, – – – JetD01, ——— JetD005, – – – JetD0025, ——— JetD005p250, – – – JetD005p2000. The arrows indicate the vortex pairing Strouhal numbers St_{pair}^{peak} in JetD02, JetD01, JetD005 and JetD0025. Measurements: ◁ Tanna,[37] ▷ Bogey *et al.*[38]

The sound pressure levels calculated at $60r_0$ from the jet nozzle exit, for $\mathrm{St} \geq 0.1$, are represented in figure 16. As previously, the strong overestimation of the acoustic levels with respect to measurements provided by Mollo-Christensen *et al.*,[35] Lush,[36] Tanna,[37] and Bogey *et al.*[38] for jets at high Reynolds numbers (see in table 4) indicates the presence of additional noise in the present initially laminar jets. The significant decrease of the levels when just adding inlet random noise of low amplitude in the pipe is also noticed. Furthermore it can be pointed out that the levels obtained for the different jets are much more scattered at an emission angle of 90° than at 30°. At the latter angle, they are even rather close to the experimental data for the four jets with thin initial shear layers. This clearly shows that the sensitivity of the sound levels to the jet exit conditions is higher in the transverse direction than in the downstream direction.

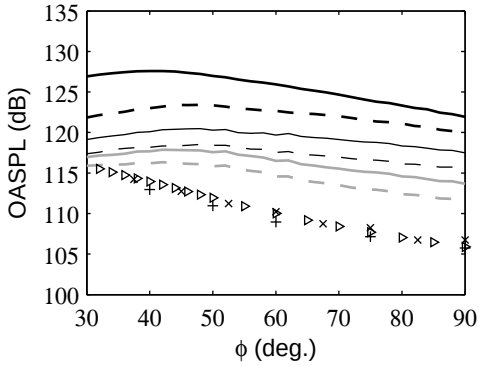

Figure 16. Sound pressure levels obtained at $60r_0$ from the jet nozzle exit, as functions of the radiation angle relative to the jet direction, for: ——— JetD02, – – – JetD01, ——— JetD005, – – – JetD0025, ——— JetD005p250, – – – JetD005p2000. Measurements: + Mollo-Christensen *et al.*,[35] × Lush,[36] ◁ Tanna,[37] ▷ Bogey *et al.*[38]

IV. Conclusion

The LES of round jets at Mach number M = 0.9 and Reynolds number $\mathrm{Re}_D = 10^5$ presented in this paper show the significant effects of the nozzle-exit boundary-layer thickness and turbulence conditions on the aerodynamic development and the acoustic field of initially laminar subsonic jets. The numerical results also agree well with measurements obtained in studies dealing separately with axisymmetric shear layers, turbulent jets or subsonic jet noise. In this way, the present simulations are used as numerical experiments under controlled conditions to reproduce and complement the experimental findings.

Decreasing the nozzle-exit boundary-layer momentum thickness δ_θ in initially laminar jets is found to especially affect the flow development. It leads in particular to an elongation of the potential core, and to a reduction of centerline turbulence intensities. For both flow features, a good agreement with experimental data available for high Reynolds number jets is thus obtained for $\delta_\theta \simeq 0.006r_0$. It then appears necessary in jet simulations to specify thin initial boundary layers. However it does not seem sufficient to get the shear-layer development and the acoustic fields that are experimentally observed for initially turbulent jets at $\mathrm{Re}_D \geq 5 \times 10^5$, namely for practical jets. Coherent vortex pairings and their strong generated noise are indeed noticed in the present initially laminar jets, whatever the exit momentum thickness may be.

The early turbulent development in initially laminar jets is dominated by processes of vortex rolling-up and pairing, which occur at frequencies related to the initial shear-layer thickness, but whose other characteristics including azimuthal properties and strength mainly depend on the initial turbulence. Therefore it turns out to be important in jet simulations to control the initial velocity disturbances, so as to impose nozzle-exit conditions as close as possible to the experimental conditions, when they are known. In the present LES, the jet shear-layer transition is for example appreciably modified by the addition of small inlet noise, leading to a weakening of the vortex pairings, and to a spectacular lowering of the far-field sound pressure levels. Such changes likely arise even for minute differences in the inflow conditions, as it can be seen from the results obtained for JetD005 and JetD005p250, which are two initially fully laminar jets with same nozzle-exit boundary-layer thickness and turbulent intensities.

Finally, the present results illustrate the importance of taking into account the issue of inflow conditions in jet simulations. This should be particularly the case in studies dealing with the prediction and the reduction of jet noise. For instance, if one aims at investigating the effects of devices such as chevrons, tabs or microjets, it should be required to ensure that the uncertainties due to the inflow conditions are lower than the variations of the sound pressure levels around −3 dB expected according to experiments.[40–43] For practical applications, vortex pairing noise appears in particular to be attenuated, which has motivated the developments of LES of initially turbulent jets.[12,44]

Acknowledgments

The authors are grateful to the Institut du Développement et des Ressources en Informatique Scientifique (IDRIS) of the French National Centre for Scientific Research (CNRS) for providing computing time, and

especially to Jean-Michel Dupays for his technical assistance.

Appendix

To improve the stability of the jet LES around the nozzle lips, the non-centered filter proposed by Berland *et al.*[23] to damp out grid-to-grid oscillations at the second row of points above boundaries has not been used but replaced by another filter with similar properties in the wavenumber space. Using this filter, a function f discretized on a uniform grid (x_i) is filtered to provide the quantity

$$\tilde{f}(x_i) = f(x_i) - \sigma \sum_{j=-2}^{8} d_j^{28} f(x_i + j\Delta x)$$

where Δx is the mesh spacing, σ is the filtering strength between 0 and 1, and d_j^{28} are the coefficients of the filter so that $d_{-2}^{28} = 0.0307159855992469$, $d_{-1}^{28} = -0.148395705486028$, $d_0^{28} = 0.312055385963757$, $d_1^{28} = -0.363202245195514$, $d_2^{28} = 0.230145457063431$, $d_3^{28} = -0.0412316564605079$, $d_4^{28} = -0.0531024700805787$, $d_5^{28} = 0.0494343261171287$, $d_6^{28} = -0.0198143585458560$, $d_7^{28} = 0.00339528102492129$, and $d_8^{28} = 0$.

References

[1]Maestrello, L. and McDaid, E., "Acoustic characteristics of a high-subsonic jet," *AIAA J.*, Vol. 9, No. 6, 1971, pp. 1058-1066.

[2]Grosche, F.-R., "Distributions of sound source intensities in subsonic and supersonic jets," AGARD-CP-131, 1974, pp. 4-1 to 4-10.

[3]Hill, W.G., Jenkins, R.C., and Gilbert, B.L., "Effects of the initial boundary-layer state on turbulent jet mixing," *AIAA J.*, Vol. 14, No. 11, 1976, pp. 1513-1514.

[4]Hussain, A.K.M.F and Zedan, M.F., "Effects of the initial condition on the axisymmetric free shear layer: Effects of the initial momentum thickness," *Phys. Fluids*, Vol. 21, No. 7, 1978, pp. 1100-1112.

[5]Hussain, A.K.M.F. and Zedan, M.F., "Effects of the initial condition on the axisymmetric free shear layer: Effects of the initial fluctuation level," *Phys. Fluids*, Vol. 21, No. 9, 1978, pp. 1475-1481.

[6]Husain, Z.D. and Hussain, A.K.M.F., "Axisymmetric mixing layer: influence of the initial and boundary conditions," *AIAA J.*, Vol. 17, No. 1, 1979, pp. 48-55.

[7]Zaman, K.B.M.Q., "Effect of initial condition on subsonic jet noise," *AIAA J.*, Vol. 23, 1985, pp. 1370-1373.

[8]Zaman, K.B.M.Q., "Far-field noise of subsonic jet under controlled excitation," *J. Fluid Mech.*, Vol. 152, 1985, pp. 83-111.

[9]Bridges, J.E. and Hussain, A.K.M.F., "Roles of initial conditions and vortex pairing in jet noise," *J. Sound Vib.*, Vol. 117, No. 2, 1987, pp. 289-311.

[10]Stanley, S.A. and Sarkar, S., "Influence of nozzle conditions and discrete forcing on turbulent planar jets," *AIAA J.*, Vol. 38, No. 9, 2000, pp. 1615-1623.

[11]Bogey, C. and Bailly, C., "Effects of inflow conditions and forcing on a Mach 0.9 jet and its radiated noise," *AIAA J.*, Vol. 43, No. 5, 2005, pp. 1000-1007.

[12]Bogey, C., Barré, S., and Bailly, C., "Direct computation of the noise generated by subsonic jets originating from a straight pipe nozzle," *Int. J. of Aeroacoustics*, Vol. 7, No. 1, 2008, pp. 1-22.

[13]Kim, J. and Choi, H., "Large eddy simulation of a circular jet: effect of inflow conditions on the near field," *J. Fluid Mech.*, Vol. 620, 2009, pp. 383-411.

[14]Colonius, T. and Lele, S.K., "Computational aeroacoustics: progress on nonlinear problems of sound generation," *Progress in Aerospace Sciences*, Vol. 40, 2004, pp. 345-416.

[15]Bodony, D.J. and Lele, S.K., "On the current status of jet noise predictions using large-eddy simulation," *AIAA J.*, Vol. 46, No. 2, 2008, pp. 364-380.

[16]Crighton, D.G., "Acoustics as a branch of fluid mechanics," *J. Fluid Mech.*, Vol. 106, 1981, pp. 261-298.

[17]Tam, C.K.W., Viswanathan, K., Ahuja, K.K., and Panda, J., "The sources of jet noise: experimental evidence," *J. Fluid Mech.*, Vol. 615, 2008, p. 253-292.

[18]Bogey, C. and Bailly, C., "Investigation of downstream and sideline subsonic jet noise using Large Eddy Simulations," *Theoret. Comput. Fluid Dynamics*, Vol. 20, No. 1, 2006, pp. 23-40.

[19]Bogey, C. and Bailly, C., "An analysis of the correlations between the turbulent flow and the sound pressure field of subsonic jets," *J. Fluid Mech.*, Vol. 583, 2007, pp. 71-97.

[20]Mohseni, K. and Colonius, T., "Numerical treatment of polar coordinate singularities," *J. Comput. Phys.*, Vol. 157, No. 2, 2000, pp. 787-795.

[21]Bogey, C. and Bailly, C., "A family of low dispersive and low dissipative explicit schemes for flow and noise computations," *J. Comput. Phys.*, Vol. 194, No. 1, 2004, pp. 194-214.

[22]Bogey, C., de Cacqueray, N., and Bailly, C., "A shock-capturing methodology based on adaptative spatial filtering for high-order non-linear computations," *J. Comput. Phys.*, Vol. 228, No. 5, 2009, pp. 1447-1465.

[23]Berland, J., Bogey, C., Marsden, O., and Bailly, C., "High-order, low dispersive and low dissipative explicit schemes for multi-scale and boundary problems," *J. Comput. Phys.*, Vol. 224, No. 2, 2007, pp. 637-662.

[24]Bogey, C. and Bailly, C., "Large Eddy Simulations of transitional round jets: influence of the Reynolds number on flow development and energy dissipation," *Phys. Fluids*, Vol. 18, No. 6, 2006, 065101.

[25]Bogey, C. and Bailly, C., "Large eddy simulations of round jets using explicit filtering with/without dynamic Smagorinsky model," *Int. J. Heat and Fluid Flow*, Vol. 27, No. 4, 2006, pp. 603-610.

[26]Bogey, C. and Bailly, C., "Turbulence and energy budget in a self-preserving round jet: direct evaluation using large-eddy simulation," *J. Fluid Mech.*, Vol. 627, 2009.

[27]Tam, C.K.W and Dong, Z., "Radiation and outflow boundary conditions for direct computation of acoustic and flow disturbances in a nonuniform mean flow., *J. Comput. Acoust.*, Vol. 4, No. 2,, 1996, pp. 175201.

[28]Bogey, C. and C. Bailly, C., "Three-dimensional non reflective boundary conditions for acoustic simulations: far-field formulation and validation test cases," *Acta Acustica*, Vol. 88, No. 4, 2002, pp. 463-471.

[29]Michalke, A., "Survey on jet instability theory," *Prog. Aerospace Sci.*, Vol. 21, 1984, pp. 159-199.

[30]Berland J., Bogey C. and Bailly C., "Numerical study of screech generation in a planar supersonic jet," *Phys. Fluids*, Vol. 19, 2007, 075105, pp. 1-14.

[31]Bogey, C., Barré, S., Juvé, D., and Bailly, C., "Simulation of a hot coaxial jet : direct noise prediction and flow-acoustics correlations," *Phys. Fluids*, Vol. 21, No. 3, 2009, 035105.

[32]Lau, J.C., Morris, P.J., and Fisher, M.J., "Measurements in subsonic and supersonic free jets using a laser velocimeter," *J. Fluid Mech.*, Vol. 93, No. 1, 1979, pp. 1-27.

[33]Arakeri, V.H., Krothapalli, A., Siddavaram, V., Alkislar, M.B., and Lourenco, L., "On the use of microjets to suppress turbulence in a Mach 0.9 axisymmetric jet," *J. Fluid Mech.*, Vol. 490, 2003, pp. 75-98.

[34]Fleury, V., Bailly, C., Jondeau, E., Michard, M., and Juvé, D., "Space-time correlations in two subsonic jets using dual-PIV measurements," *AIAA J.*, Vol. 46, No. 10, 2008, pp. 2498-2509.

[35]Mollo-Christensen, E., Kolpin, M.A., and Martucelli, J.R., "Experiments on jet flows and jet noise far-field spectra and directivity patterns," *J. Fluid Mech.*, Vol. 18, 1964, pp. 285-301.

[36]Lush, P.A., "Measurements of subsonic jet noise and comparison with theory," *J. Fluid Mech.*, Vol. 46, No. 3, 1971, pp. 477-500.

[37]Tanna, H.K., "An experimental study of jet noise. Part I: Turbulent mixing noise," *J. Sound Vib.*, Vol. 50, No. 3, 1977, pp. 405-428.

[38]Bogey, C., Barré, S., Fleury, V., Bailly, C., and Juvé, D., "Experimental study of the spectral properties of near-field and far-field jet noise," *Int. J. of Aeroacoustics*, Vol. 6, No. 2, 2007, pp. 73-92.

[39]Zaman, K.B.M.Q. and Hussain, A.K.M.F., "Vortex pairing in a circular jet under controlled excitation. Part 1. General jet response," *J. Fluid Mech.*, Vol. 101, No. 3, 1980, pp. 449-491.

[40]Saiyed, N.H., Mikkelsen, K.L., and Bridges, J.E., "Acoustics and thrust of quiet separate-flow high-bypass-ratio nozzles," *AIAA J.*, Vol. 41, No. 3, 2003, pp. 372-378.

[41]Callender, B., Gutmark, E., and Martens, S., "Far-field acoustic investigation into chevron nozzle mechanisms and trends," *AIAA J.*, Vol. 43, No. 1, 2005, pp. 87-95.

[42]Alkislar, M.B., Krothapalli, A., and Butler, G.W., "The effect of streamwise vortices on the aeroacoustics of a Mach 0.9," *J. Fluid Mech.*, Vol. 578, 2007, pp. 139-169.

[43]Castelain, T., Sunyach, M., Juvé, D., and Béra, J.-C., "Jet-noise reduction by impinging microjets: an acoustic investigation testing microjet parameters," *AIAA J.*, Vol. 46, No. 5, 2008, pp. 1081-1087.

[44]Uzun, A. and Hussaini, M., "Investigation of high frequency noise generation in the near-nozzle region of a jet using large eddy simulation," *Theoret. Comput. Fluid Dynamics*, Vol. 21, No. 4, 2007, pp. 291-321.